Neuron
Report

Representation of Geometric Borders in the Developing Rat

Tale L. Bjerknes,[1] Edvard I. Moser,[1] and May-Britt Moser[1,*]
[1]Kavli Institute for Systems Neuroscience, Norwegian University of Science and Technology, NO-7489 Trondheim, Norway
*Correspondence: maybm@ntnu.no
http://dx.doi.org/10.1016/j.neuron.2014.02.014

SUMMARY

Local space is represented by a number of functionally specific cell types, including place cells in the hippocampus and grid cells, head direction cells, and border cells in the medial entorhinal cortex (MEC). These cells form a functional map of external space already at the time when rat pups leave the nest for the first time in their life, at the age of 2.5 weeks. However, while place cells have adult-like firing fields from the outset, grid cells have irregular and variable fields until the fourth week, raising doubts about their contribution to place cell firing at young age. Recording in MEC of juvenile rats, we show that, unlike grid cells, border cells express adult-like firing fields from the first days of exposure to an open environment, at postnatal days 16–18. Thus, spatial signals from border cells may be sufficient to maintain spatially localized firing in juvenile hippocampal place cells.

INTRODUCTION

An animal's position in the local environment is monitored by a spectrum of functionally specific cell types in the hippocampus and the adjacent parahippocampal areas, particularly the MEC. In the hippocampus, place cells fire selectively when the animal visits one or a few specific locations of the local environment (O'Keefe and Dostrovsky, 1971). In the MEC, grid cells fire at multiple locations that, for each cell, define a hexagonal grid that tessellates the entire space available to the animal (Hafting et al., 2005). Although the majority of cells in superficial MEC layers are grid cells (Sargolini et al., 2006), these cells intermingle with border cells, which fire whenever the animal comes close to one or several local geometric boundaries, such as the walls of the recording enclosure (Savelli et al., 2008; Solstad et al., 2008). In layer III and deeper MEC layers, grid cells (Sargolini et al., 2006) also mix with head direction cells, which fire only when the animal faces a given direction (Ranck, 1985; Taube et al., 1990).

The presence of multiple spatial cell types within the same brain system raises questions about their interrelationships. Place cells are probably generated from spatial inputs from the entorhinal cortex, the main cortical source of input to the hippocampus. The abundance of grid cells in the superficial layers of MEC points to grid cells as a likely source for the place cell signal. In several early models, place cell formation was explained by a Fourier mechanism in which periodic firing fields from grid cells with different grid spacing were linearly combined to generate single fields in hippocampal target neurons (O'Keefe and Burgess, 2005; Fuhs and Touretzky, 2006; McNaughton et al., 2006; Solstad et al., 2006). This possibility has been challenged, however, by the observation that place cells mature faster than grid cells in young animals (Langston et al., 2010; Wills et al., 2010). When rat pups leave the nest for the first time at postnatal day 16 or 17 (P16–P17), many place cells already have sharply confined firing fields similar to those of adult animals. In contrast, grid cells are far from fully developed. Firing fields are irregular and variable in size and shape and although some spatial periodicity can be observed in some neurons, adult-like patterns do not appear until approximately 1.5 weeks later, near the age of 4 weeks. The lack of sharply confined grid outputs in the 2.5- to 4-week-old nervous system has raised the possibility that juvenile place cells receive spatial information from other functional cell populations, such as the border cells of the MEC. The present study was designed to test whether functional border cells are present at this developmental stage. We find that border cells have adult-like firing fields from the very first days of outbound navigation, at 2.5 weeks of age.

RESULTS

Neural activity was recorded from the MEC of nine female and 11 male juvenile Long-Evans rats and from four adult male rats (Table S1 available online). The pups were implanted with tetrodes from P14, around the time when the eyelids unseal. On the subsequent day, the tetrodes were moved toward the superficial layers of MEC (Figures 1A and S1). Once single neurons could be isolated at appropriate depths, the pups were placed in a 70 cm × 70 cm arena with 50 cm high walls and spike activity was recorded. One rat was introduced to the box already on P15, 11 rats started on P16, and one on P17. Seven rats started at P24–P26.

MEC cells could be recorded from P16 in three rats, from P17 in five rats, from P18 in three rats, and from P19 in two rats. The rats explored the entire box by the end of the first age block (P16–P18). There was little change in running pattern during subsequent age blocks (speed: P16–P18: 9.6 ± 0.3 cm/s; P34–P36: 11.0 ± 0.7 cm/s; adult: 12.2 ± 0.2 cm/s, ANOVA: $F(7,75) = 2.41$, $p < 0.05$; coverage: 90.5% ± 0.3%, 92.4% ± 1.6%, and 91.6% ± 0.6%, respectively, $F(7,75) = 0.61$, $p = 0.80$). Average firing rate for all cells increased significantly with age (P16–P18: 1.17 ± 0.08 Hz; P34–36: 1.29 ± 0.11 Hz; adults: 1.72 ± 0.10 Hz; $F(7(1,105) = 3.12$, $p < 0.005)$).

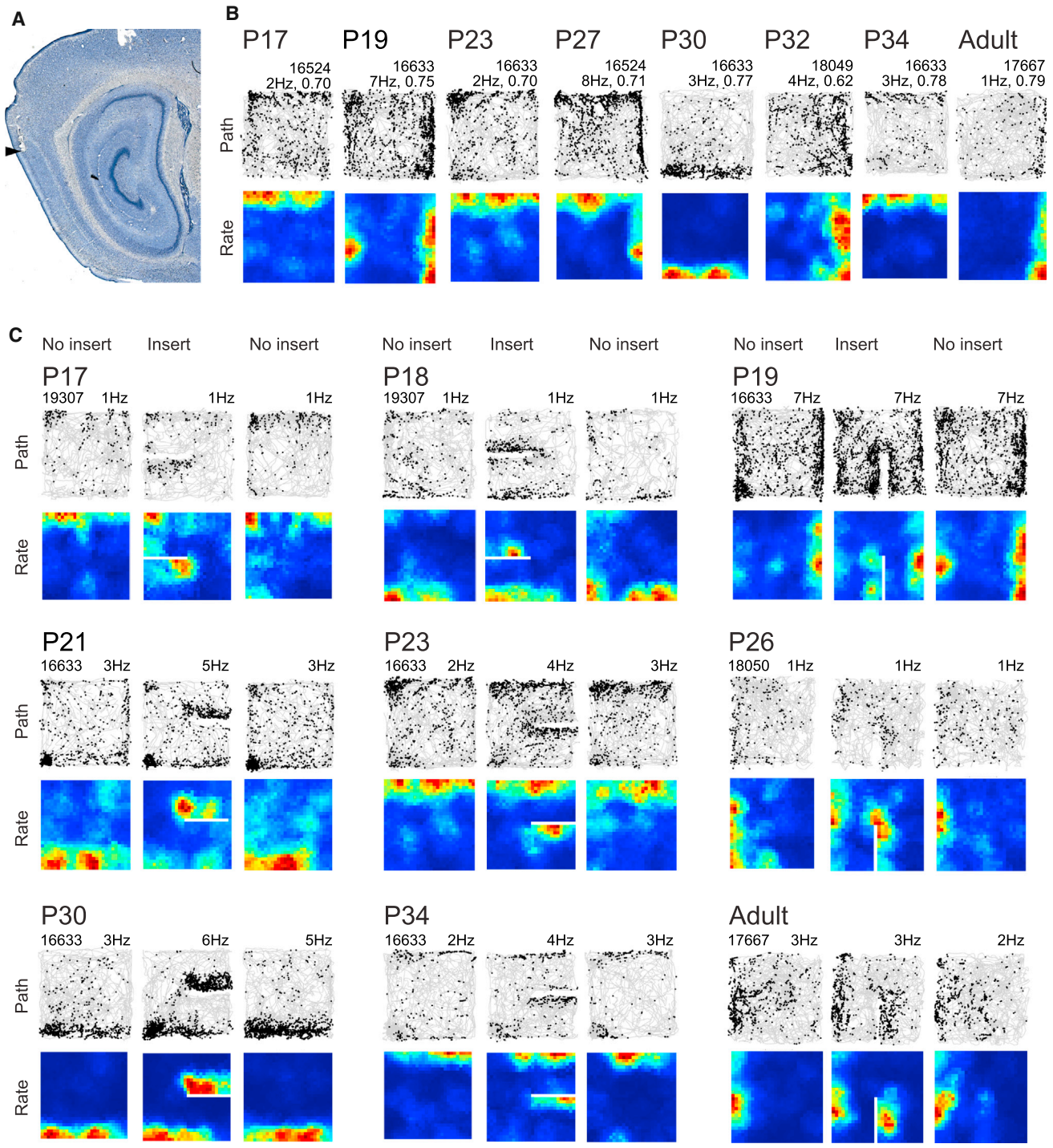

Figure 1. Examples of Border Cells in MEC of Juvenile Rats

(A) Nissl-stained sagittal brain section with a representative recording location (arrowhead) in layer II of MEC. Data were recorded between P16 and P26 in this rat. The rat was killed on P26. (B) Development of border cells from P17 to P34 and adult age. Top row: trajectory with spike positions indicated. Bottom row: rate maps color-coded from dark blue (0 Hz) to dark red (peak firing rate). Animal identities (five digits), as well as peak firing rates and border scores, are indicated at the top. (C) Trajectory maps and rate maps for border cells before and after insertion of a discrete wall (P17–P34 and adult age). Animal identities (five digits) and peak firing rates are indicated. Three consecutive trials are shown; the wall was inserted on the middle trial in parallel with the border cell's original firing field.

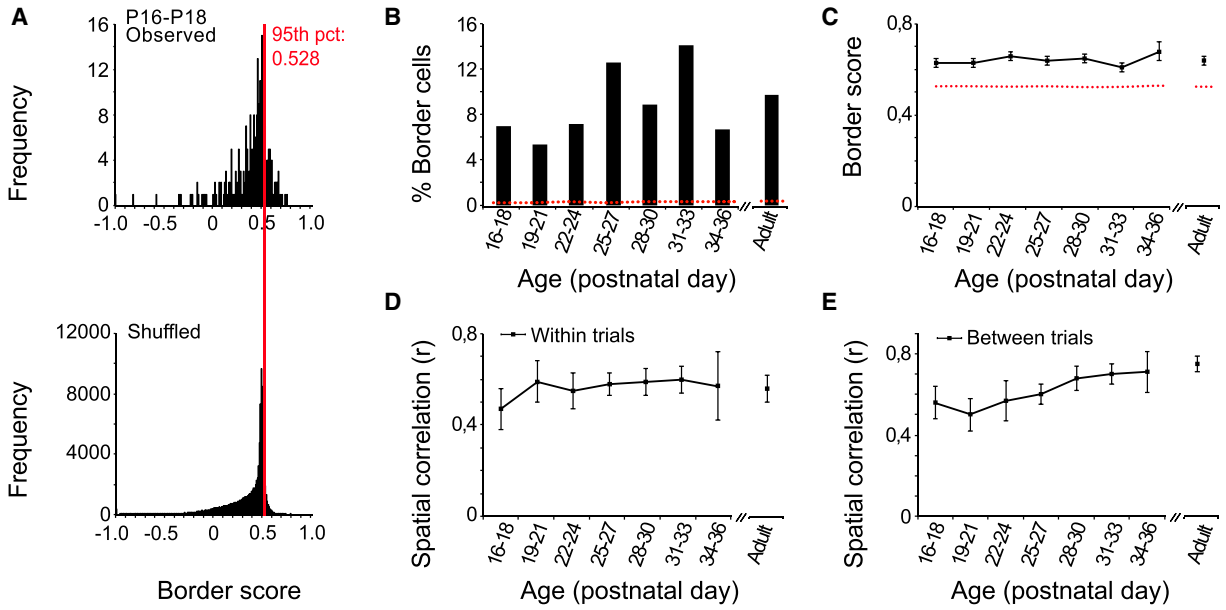

Figure 2. Development of Border Cells

(A) Distribution of border scores in observed data (top) and shuffled versions of the same data (bottom) at P16–P18. Red line indicates 95th percentile for border score in the shuffled data. (B) Percentage of border cells passing dual 95th percentile criterion for border scores and spatial information as a function of age. Red stippled line indicates proportion of cells expected to pass the dual criterion by chance (0.2%–0.4%). (C) Border scores as a function of age for all border cells (means ± SEM); 95th percentile of shuffled data is indicated by a red stippled line. (D and E) Spatial correlation within trials (D) and between trials (E) as a function of age for all border cells (means ± SEM).

Border Cells

In adult rats, MEC contains a small but distinct population of border cells (Savelli et al., 2008; Solstad et al., 2008). We identified such cells by computing, for each cell, the difference between the maximal length of a single wall touching on a single firing field and the average distance of this field from the wall, divided by the sum of those values (Solstad et al., 2008). A cell was classified as a border cell if this border score, as well as the spatial information content of the cell, exceeded the 95th percentiles of border and spatial information scores for shuffled data from all cells in the respective age group (Figure 2A; Experimental Procedures).

Nine out of 128 MEC cells (7.0%) passed the classification criterion in the youngest age group (P16–P18; Figures 1B, 2B, and S2). This percentage is significantly larger than in the shuffled data, where only 0.2% of the cells passed the 95th criteria for both border scores and spatial information (Figure 2B; $Z = 16.4$, $p < 0.001$). In subsequent age blocks, the percentage of border cells fluctuated between 5% and 14%, all significantly above the chance level (0.2%–0.4%; $p < 0.001$) and with no systematic increase across age blocks. The percentage of border cells was not different between juvenile animals (P16–P36) and adult animals (8.5% in the juvenile group and 9.8% in the adult group; $Z = 0.65$, $p = 0.52$). There was no age-related increase in border scores for cells that passed the criterion (Figure 2C; $F(7,98) = 1.06$, $p = 0.39$). Most cells had border fields along a single wall; 26 had fields along two walls and one had fields along all four walls. Cells with fields along two walls appeared in all age groups except P34–P36. The cell with four fields was from an adult rat. The number of border fields per cell did not increase with age ($F(7,90) = 1.19$, $p = 0.32$).

Border cells had sharply defined firing fields in all age groups but the spatial discreteness of the fields increased with age (spatial coherence at P16–P18 and in adults: 0.27 ± 0.05 and 0.48 ± 0.05, respectively; spatial information: 0.46 ± 0.04 and 0.65 ± 0.06; ANOVA for all age groups, spatial coherence: $F(7,98) = 2.39$, $p = 0.03$; spatial information: $F(7, 98) = 2.54$, $p = 0.02$). Field size decreased with age ($F(7,98) = 2.96$, $p < 0.01$). The stability of the border fields did not increase with age (Figures 2D and 2E; within trials: $F(7,98) = 0.30$, $p = 0.95$; between trials: $F(7,96) = 1.86$, $p = 0.09$) nor did the average firing rate (all border cells, 0.66 ± 0.15 Hz at P16–P18; 0.58 ± 0.12 Hz at P34–P36; 0.90 ± 0.12 Hz in adults; $F(7,98) = 0.83$, $p = 0.57$).

The functional identity of border cells was verified on separate experimental trials by placing a wall centrally in the recording box, in parallel with the wall that maintained the firing field on the initial baseline trial. In adult rats, this procedure nearly always evokes a new border field on the distal side of the wall insert, on the side that faces away from the original field (Barry et al., 2006; Solstad et al., 2008). A similar response was observed in border cells from the youngest animals (Figure 1C and Figure S3). At all ages, the firing rate on the distal side of the new wall (10 cm or closer; Figure 3A) increased by a factor of 2 or more, compared to the baseline trial (Figures 3B and 3C). Removing the wall reversed the rate (Figures 1C and S3). There was no corresponding increase on the proximal side of the wall (Figures 1C, 3B, 3C, and S3). The increase on the distal side was significant across the entire age range (repeated-measures ANOVA for absolute

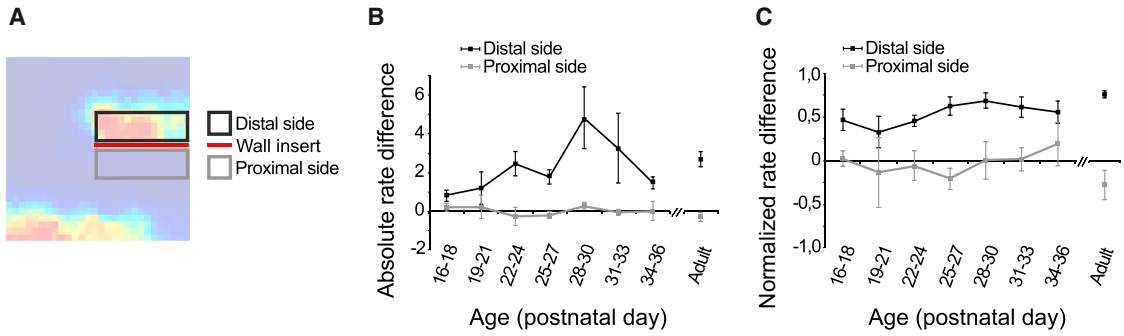

Figure 3. Response to Insert of New Wall in the Recording Box

(A) Schematic indicating procedure to estimate response to insertion of a new wall (red line). Firing rates were measured in a 10-cm-wide area on the proximal side (gray rectangle) and the distal side (black rectangle) of the wall. Proximal and distal were defined relative to the location of the peripheral border field. The rate map of a cell with an original field along the south wall is indicated. (B) Absolute change in firing rate on the distal and proximal sides of the wall as a function of age (difference between rate in the presence of the wall and rate in the same area on the baseline trial; means ± SEM). (C) Normalized change in firing rate on the distal and proximal sides of the wall (means ± SEM). Firing rate was normalized by dividing the difference between firing rates in the rectangle before and after wall insert by the sum of these rates. Note that normalized distal firing rate is elevated equally at all ages, suggesting that the lower absolute differences in the youngest groups in (B) reflect lower average firing rates.

rate difference with age and trial as factors: trial: $F(1,36) = 44.8$, $p < 0.001$; age: $F(7,36) = 1.92$, $p = 0.10$; trial × age: $F(7,36) = 1.94$, $p = 0.09$). There was no effect of the wall insert on firing rates on the proximal side (all Fs < 1). Thus, border cells with adult-like properties are present in MEC from the very first days of outbound navigation.

Grid Cells

Grid cells matured more slowly than border cells. As in previous studies with different cohorts (Langston et al., 2010; Wills et al., 2010), MEC cells failed to express adult-like hexagonal firing patterns until the rats reached approximately 4 weeks of age, despite the presence of adult-like border cells in the same animals. In the youngest groups, the MEC contained cells with multiple firing fields, many of which showed some rudimentary periodic structure, but the firing pattern was more variable than in older animals (Figures 4A and S4). The presence of grid structure was quantified by calculating, for each cell, a grid score based on rotational symmetry in the cell's spatial autocorrelogram (Sargolini et al., 2006; Langston et al., 2010). Cells were classified as grid cells if they had grid scores and spatial information scores that each exceeded the 95th percentile of grid scores and spatial information scores, respectively, from a shuffled distribution for the respective age group (Figure 4B). Two out of 128 cells (1.6%) passed this dual criterion in the P16–P18 group (Figure 4C). The fraction was slightly but significantly larger than in the shuffled data, where 0.2% of the cells passed both criteria ($Z = 3.3$, $p = 0.001$). In the P19–P21 group, seven out of 185 cells (3.8%) passed the dual criterion (chance level: 0.2%–0.3%; $Z = 8.1$, $p < 0.001$). At subsequent ages, the percentage of grid cells increased slowly (all $p < 0.001$). The percentage of cells that passed the grid cell criterion was significantly larger in the adult group than in the entire group of young animals (P16–P36; $Z = 9.02$, $p < 0.001$). Cells that passed the criterion for grid cells showed a significant increase in grid scores across age blocks (Figure 4D; $F(7, 82) = 3.858$, $p = 0.001$). The stability of the grid fields increased significantly with age (Figures 4E and 4F; within trials: $F(7, 82) = 6.1$, $p < 0.001$; between trials: $F(7, 82) = 11.1$, $p < 0.001$); as did the spatial discreteness of the firing fields (ANOVA for spatial coherence: $F(7, 82) = 2.9$, $p < 0.01$; spatial information: $F(7, 82) = 2.3$, $p < 0.05$).

Head Direction Cells

Head direction cells were present in all age groups, in agreement with previous studies (Langston et al., 2010; Wills et al., 2010). Directional modulation was expressed by the mean vector length of the cell's firing rate. Cells were classified as head direction cells if the mean vector length exceeded the 95th percentiles of shuffled distributions for both directional information and mean vector length. Fifty-five out of 128 cells (43.0%) passed the criterion for head direction cells in the P16–P18 group. This fraction is significantly larger than in the shuffled data, where 0.9% of the cells passed both criteria ($Z = 49.0$, $p < 0.001$). The percentage of head direction cells did not increase with age (P19–P21: 40.5%; P22–P24: 34.5%; P25–P27: 29.6%; P28–P30: 25.3%; P31–P33: 34.1%; P34–P36: 35.0%, and adult: 48.8%). Cells that passed the criterion for head direction cells showed a significant increase in mean vector length across age blocks ($F(7, 424) = 4.3$, $p < 0.001$). The stability of directional tuning increased significantly (within trials: $F(7, 421) = 3.8$, $p < 0.001$; between trials: $F(7, 406) = 3.6$, $p = 0.001$).

DISCUSSION

The key finding of this study is that entorhinal border cells are already present when rat pups make their first navigational experiences. When rat pups leave the nest at the age of 2.5 weeks, many MEC cells fire selectively along one or several environmental boundaries. Although the sharpness and the stability of border fields show some increase from young to adult age, the basic properties of border cells appear to be present from the outset. In particular, when a wall is inserted in parallel with the original peripheral firing field, the cells develop new firing fields along the insert, just as in adult rats. Head direction cells

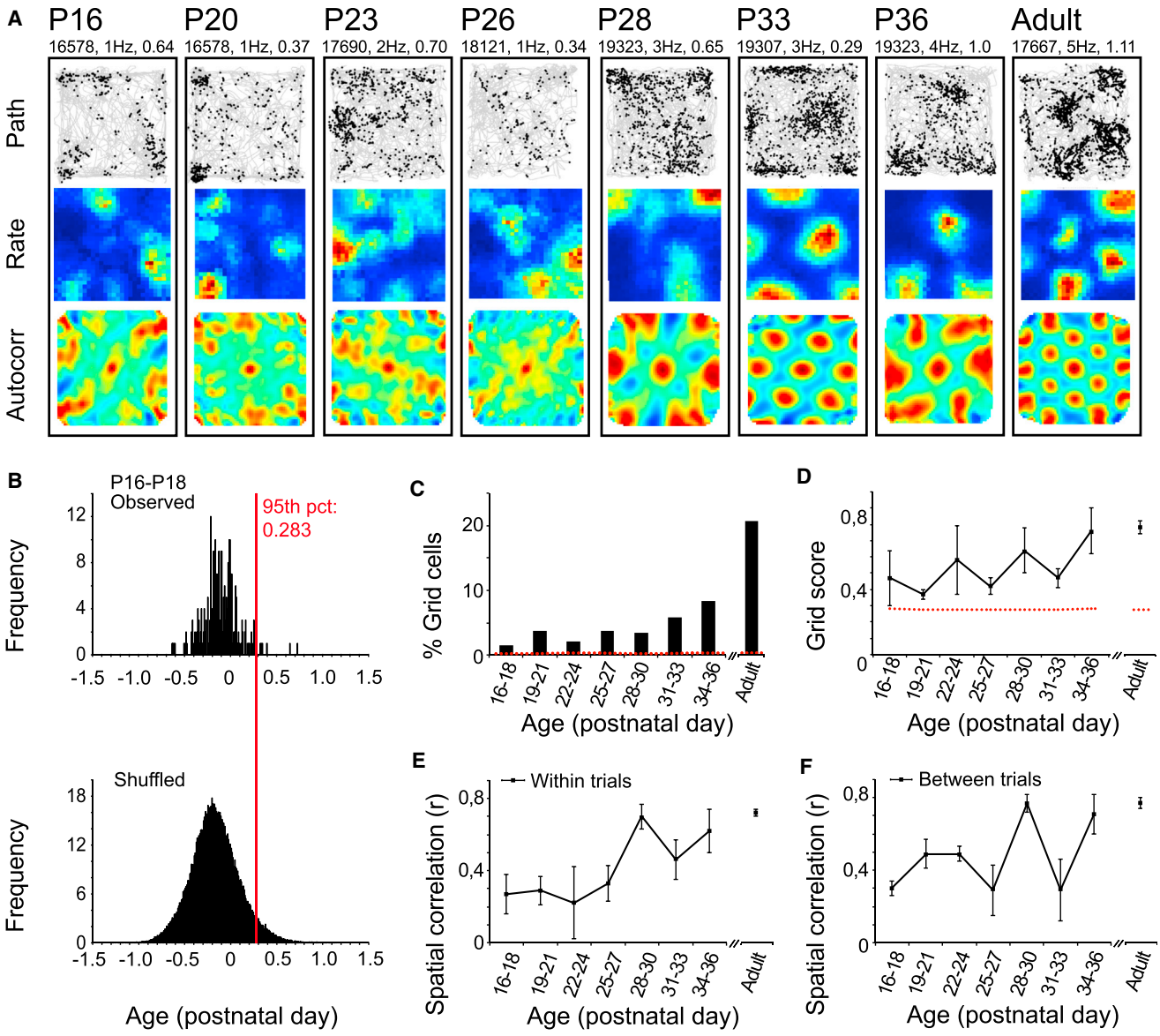

Figure 4. Development of Grid Cells

(A) Development of grid cells. Animal identities, peak firing rates, and grid scores are indicated at the top. Top row: trajectory with spike positions. Middle row: color-coded rate maps (as in Figure 1B). Bottom row: color-coded spatial autocorrelograms (dark blue is −1, dark red is +1). (B) Distribution of grid scores in the observed data at P16-P18 (top) and in shuffled versions of the same data; 95th percentile of the shuffled data is indicated by a red line. (C) Percentage of grid cells passing dual 95th percentile criterion for grid scores and spatial information as a function of age. Red stippled line indicates proportion of cells expected to pass the dual criterion by chance (0.2%–0.3%). (D) Grid scores as a function of age for all grid cells (means ± SEM; 95th percentile of shuffled data indicated by red stippled line). (E) Within-trial spatial correlations as a function of age for all grid cells (means ± SEM). (F) Between-trial spatial correlations as a function of age for all grid cells (means ± SEM).

were also present from the outset. In contrast, grid cells, recorded in the same animals, matured slowly, showing only minimal spatial periodicity during the first week of outbound exploration. The slow maturation of the grid cells and the fast expression of directional modulation confirm previous observations (Langston et al., 2010; Wills et al., 2010).

The presence of border cells in the immature MEC has implications for mechanisms of place cells. Place cells receive the majority of their cortical inputs from the entorhinal cortex (Witter and Amaral, 2004). Spatial signals are thought to originate primarily in the medial part of the entorhinal cortex (Fyhn et al., 2004; Hafting et al., 2005; Hargreaves et al., 2005). The fact that the majority of hippocampus-projecting spatially modulated cells in this area are grid cells (Sargolini et al., 2006; Zhang et al., 2013) has raised the possibility that place cells emerge by transformation of inputs from grid cells. One class of models relies on linear summation of impulses from cells with different grid spacing but similar grid phase and grid orientation (O'Keefe

and Burgess, 2005; Fuhs and Touretzky, 2006; McNaughton et al., 2006; Solstad et al., 2006). However, these models cannot readily account for the fact that place cells mature faster than grid cells in developing animals (Langston et al., 2010; Wills et al., 2010), although with the addition of local circuit mechanisms and Hebbian plasticity, weakly modulated and irregular spatial inputs would in principle be sufficient to generate discrete and stable place fields (Rolls et al., 2006; de Almeida et al., 2009; Savelli and Knierim, 2010; Monaco and Abbott, 2011). The present findings point to border cells as an alternative source of spatial information to the hippocampus of young animals, possibly with head direction cells as an additional source of modulation. Only a small fraction of the entorhinal cell population has properties defining them as border cells but retrograde labeling suggests that the hippocampal projections of these cells may be as dense as those of the more slowly developing grid cells (Zhang et al., 2013). The present study, in conjunction with the retrograde labeling study, suggests that these projections may be present from young age. Place cells may thus be formed by inputs from both grid cells and border cells but in the immature nervous system the border cells may provide the most reliable spatial inputs. In adult animals, border cells may provide sufficient spatial input to generate spatial firing fields in hippocampal neurons under conditions when the periodicity of the grid cells is compromised (Koenig et al., 2011).

Our observations revitalize the idea that spatially localized firing is generated in place cells based on inputs from cortical cells with firing fields defined by their proximity to geometric boundaries (O'Keefe and Burgess, 1996). Computational models have shown that such cells may be sufficient to generate place fields of any shape and size at any location of the environment (Barry et al., 2006; Hartley et al., 2000). One caveat, however, is that while these models rely on inputs from cells with fields at a continuum of distances from the geometric boundaries of the environment ("boundary vector cells"), recordings in the MEC have so far only identified cells with fields that line up along the walls of the environment or very close to them ("border/boundary" cells; Savelli et al., 2008; Solstad et al., 2008; Zhang et al., 2013). Cells with more extended fields have been reported in the subiculum (Barry et al., 2006; Lever et al., 2009), but the subiculum has only very limited projections back to the hippocampus (Witter and Amaral, 2004). Border cells may thus contribute to localized firing in place cells with fields at or near the periphery of the environment, whereas central place fields may rely more on other cell types, such as grid cells, which fire with high spatial precision throughout the arena. An implication of this possibility would be that in young animals with immature grid cells, place cells may be less discrete and less stable in the center of an open field than along the boundaries. Preliminary data support this prediction (Cacucci et al., 2013, Soc. Neurosci., abstract) but definite tests may require larger open spaces than the ones used to estimate spatial firing in rat pups in the present study.

EXPERIMENTAL PROCEDURES

Subjects

Neural activity was recorded from MEC in 24 Long-Evans rats (9 female, 15 male). Twenty of the rats were implanted between P13 and P25 and tested between P16 and P36. Individual rats were tested across multiple days (P16–P36: 3–12 recording days, adult: 5–29 days). Four male rats were implanted as adults (3–4 months of age). All young animals were bred in-house; two adults were imported from Charles River Laboratories. All experiments were approved by the National Animal Research Authorities in Norway.

Postnatal day 0 (P0) was defined as the first day a new litter was observed. Pregnant mothers were checked several times per day (8 a.m.–8 p.m.). Rat pups lived with mother and siblings in transparent Plexiglas cages (55 × 45 × 35 cm), enriched with plastic toys, small fabric houses, and paper. At P21, they were weaned from their mother and housed in same-sex groups in transparent plastic cages (46 cm × 40 cm × 40 cm). A maximum of four animals from each litter were used for experiments. Litter sizes did not exceed eight. Juvenile animals had free access to food and water; adults were mildly food deprived. All rats were held on a 12 hr light/12 hr dark schedule. Testing occurred in the dark phase.

Surgery

The rats were anesthetized in an induction chamber with 5% isoflurane and 2,000 ml/min room air, reduced to 3% with 1,200 to 1,400 ml/min room air at the start of surgery. The animal received subcutaneous injections of bupivacaine (Marcaine) and carprofen (Rimadyl; in pups) or buprenorphine (Temgesic; in adults). The concentration of isoflurane was gradually reduced to 1%. Depth of anesthesia was monitored by testing tail and pinch reflexes as well as breathing.

Anesthetized rats were implanted with a single microdrive with four tetrodes cut flat to the same level. Each tetrode was made of a 17 μm polyimide-coated platinum-iridium wire. The tetrodes were platinum plated to reduce impedances to ~200 kΩ at 1 kHz. A jeweler's screw served as a ground electrode. Tetrodes were implanted in MEC at an angle of 7°–9° in the posterior-to-anterior direction in the sagittal plane, starting 0.3–0.4 mm in front of the transverse sinus and 4.5–4.7 mm lateral to the midline. Initial tetrode depth was 1.8 mm ventral to the dura. The implant was secured to the skull with jeweller's screws and dental cement. After the rat woke up from the anesthesia, the pup was placed back to mother and siblings. The implant was wrapped in surgical tape.

Data Collection

Data collection started the day after surgery. The rat rested on a flower pot covered by towels while signals were checked. The animal was connected to the recording system via an AC-coupled unity-gain operational amplifier close to the head, using a light-weight counterbalanced 16-channel cable from the implant to the amplifier. In all age groups, including adults, tetrodes were lowered in steps of 50 μm (maximum 200 μm per day) until single neurons were isolated. The rat was then placed inside the recording arena. After recording, the tetrodes were moved further. Each session lasted a maximum of 2 hr.

Recorded signals were amplified 6,000 to 14,000 times and band-pass filtered between 0.8 and 6.7 kHz. Triggered spikes were stored to disk at 48 kHz with a 32 bits time stamp. An overhead camera recorded the position of one large and one small light-emitting-diode (LED) on the head stage. The diodes were positioned 6 cm apart and aligned with the body axis.

Apparatus and Training Procedures

Data were recorded in a square enclosure (70 cm × 70 cm × 50 cm) with walls covered by black adhesive plastic and a white plastic cue card (35 cm × 50 cm) at a constant location. The box was in a constant location. Running was maintained by crumbs of chocolate or vanilla biscuits. Each session consisted of two to four 15 min trials. Between trials, the pups rested 2–20 min in the flower pot and occasionally 20 additional min in a small cage with bedding and water. The cable was not unplugged between trials. When a putative border cell was identified on the first trial, a wall (35 cm × 1 cm × 50 cm) was inserted centrally in the box on the next trial. The wall was placed in parallel with the peripheral wall along which the cell had its initial border field. Floor and walls were washed with soapy water between trials.

Analysis of Spike and Position Data

Cell classification was performed manually using graphical cluster cutting tools as described previously (Langston et al., 2010). Putative interneurons

(identified by average rate and spike amplitude width) were not included in any analysis. The rat's position was tracked via LEDs on the rat's headstage. All data were speed filtered (epochs with speed lower than 2.5 cm/s or higher than 100 cm/s were deleted). Position data were smoothed using a 21-sample boxcar window filter (400 ms, 10 samples on each side). If the rat visited less than 80% of the total number of position bins (each 2.5 cm × 2.5 cm), the trial was excluded.

Rate Maps

Firing rate distributions were determined by counting the number of spikes and time spent in each 2.5 cm × 2.5 cm bin, using a boxcar average over the surrounding 5 × 5 bins (Langston et al., 2010). To improve the tradeoff between blurring error and sampling error, an adaptive smoothing method was used on the rate maps before field size and border scores were estimated (Skaggs et al., 1996; Langston et al., 2010).

Spatial information content for the rate map, in bits per spike, was calculated as

$$\text{information content} = \sum_i p_i \frac{\lambda_i}{\lambda} \log_2 \frac{\lambda_i}{\lambda}$$

where λ_i is the mean firing rate of a unit in the i-th bin, λ is the overall mean firing rate, and p_i is the probability of the animal being in the i-th bin (occupancy in the i-th bin/total recording time) (Skaggs et al., 1993). Spatial coherence was estimated as the mean correlation between firing rate of each bin and mean firing rate in the eight adjacent bins (Muller and Kubie, 1989).

Analysis of Border Cells

Border cells were identified by computing, for each cell with an average rate above 0.2 Hz, the difference between the maximal length of a wall touching on any single firing field of the cell and the average distance of the field from the nearest wall, divided by the sum of those values. Border scores thus ranged from –1 for cells with infinitely small central fields to +1 for cells with infinitely narrow fields that lined up perfectly along the entire wall. Firing fields were defined as collections of neighboring pixels with firing rates higher than 20% of the cell's peak firing rate and a size of at least 200 cm^2.

Border cells were defined as cells with border scores exceeding chance level, determined for each age group by a shuffling procedure. For each permutation trial, the entire sequence of spikes fired by the cell was time shifted along the animal's path by a random interval between 20 s and the total trial length minus 20 s, with the end of the trial wrapped to the beginning. A rate map was then constructed, and spatial information content and border score were determined. Distributions of spatial information and border scores were generated for the entire set of permutations from all cells in the sample (400 permutations per cell), and 95th percentiles were determined for spatial information as well as border scores. Cells were defined as border cells if (1) the spatial information content in the recorded data was higher than the corresponding 95th percentile in the shuffled data, and (2) the border score from the recorded data was higher than the 95th percentile for border scores in the shuffled data. Border cell stability was estimated by calculating the spatial correlation between first and second half of the trial and between consecutive trials in the same session.

Analysis of Grid Cells

The periodicity of the rate maps was evaluated for all cells with average rates above 0.2 Hz by calculating a spatial autocorrelation map for each smoothed rate map (Sargolini et al., 2006). The degree of spatial periodicity was determined for each recorded cell by taking a central circular sample of the autocorrelogram, with the central peak excluded, and comparing rotated versions of this sample (Sargolini et al., 2006; Langston et al., 2010). The Pearson correlation of the circular sample with its rotation in α degrees was obtained for angles of 60° and 120° on one side and 30°, 90°, and 150° on the other. The cell's grid score was defined as the minimum difference between any of the elements in the first group and any of the elements in the second.

Grid cells were identified as cells in which (1) spatial information content and (2) rotational-symmetry-based grid scores exceeded the 95th percentiles of distributions of spatial information content and grid scores, respectively, in shuffled versions of the same data. Shuffling was performed as for border cells, with 400 permutation trials per recorded cell. Grid cell stability was estimated by calculating the spatial correlation between the first and the second half of individual trials or between consecutive trials.

Analysis of Head Direction Cells

The rat's head direction was calculated for each tracker sample from the projection of the relative position of the two LEDs onto the horizontal plane. The directional tuning function for each cell was obtained by plotting the firing rate as a function of the rat's directional heading. Maps for number of spikes and time were smoothed individually with 14.5° mean window filter (14 bins on each side). Directional information was calculated for each cell as for spatial information content, with λ_i as the mean firing rate of a unit in the i-th bin, λ as the overall mean firing rate, and p_i as the frequency at which the animal's head pointed in the i-th directional bin. Directional stability was estimated by correlating firing rates between the first and second half of the trial or between consecutive trials.

Directional tuning was estimated by computing the length of the mean vector for the circular distribution of firing rate. Head direction cells were identified as cells in which (1) directional information content and (2) mean vector length exceeded the 95th percentiles of distributions of directional information content and mean vector lengths, respectively, in shuffled versions of the same data. Shuffling was performed as for border cells, with 400 permutation trials per recorded cell.

Histology and Reconstruction of Recording Positions

The tetrodes were not moved after the last recording day. The rat received an overdose of Pentobarbital and was perfused with an intracardial injection of 9% saline, followed by 4% formaldehyde. The brain was stored in 4% formaldehyde, after which it was quickly frozen and cut in 30 μm sagittal slices, mounted on glass, and stained with cresyl violet. The final position of the tip of each tetrode was identified on digital pictures of the brain sections.

SUPPLEMENTAL INFORMATION

Supplemental Information includes four figures and one table and can be found with this article online at http://dx.doi.org/10.1016/j.neuron.2014.02.014.

ACKNOWLEDGMENTS

We thank N. Dagslott for help with experiments; V. Frolov and R. Skjerpeng for programming; M.P. Witter for advice on histology; N.K. Eikeland for help with figures; and A.M. Amundsgård, K. Haugen, E. Henriksen, K. Jenssen, E. Kråkvik, and H. Waade for technical assistance. Supported by the Kavli Foundation, a student research grant from the Faculty of Medicine at the Norwegian University of Science and Technology, an Advanced Investigator Grant from the European Research Council ("ENSEMBLE"–grant agreement 268598), and a Centre of Excellence grant and a FRIPRO grant from the Research Council of Norway.

Accepted: February 6, 2014
Published: March 6, 2014

REFERENCES

Barry, C., Lever, C., Hayman, R., Hartley, T., Burton, S., O'Keefe, J., Jeffery, K., and Burgess, N. (2006). The boundary vector cell model of place cell firing and spatial memory. Rev. Neurosci. *17*, 71–97.

de Almeida, L., Idiart, M., and Lisman, J.E. (2009). The input-output transformation of the hippocampal granule cells: from grid cells to place fields. J. Neurosci. *29*, 7504–7512.

Fuhs, M.C., and Touretzky, D.S. (2006). A spin glass model of path integration in rat medial entorhinal cortex. J. Neurosci. *26*, 4266–4276.

Fyhn, M., Molden, S., Witter, M.P., Moser, E.I., and Moser, M.B. (2004). Spatial representation in the entorhinal cortex. Science *305*, 1258–1264.

Hafting, T., Fyhn, M., Molden, S., Moser, M.B., and Moser, E.I. (2005). Microstructure of a spatial map in the entorhinal cortex. Nature *436*, 801–806.

Hargreaves, E.L., Rao, G., Lee, I., and Knierim, J.J. (2005). Major dissociation between medial and lateral entorhinal input to dorsal hippocampus. Science *308*, 1792–1794.

Hartley, T., Burgess, N., Lever, C., Cacucci, F., and O'Keefe, J. (2000). Modeling place fields in terms of the cortical inputs to the hippocampus. Hippocampus *10*, 369–379.

Koenig, J., Linder, A.N., Leutgeb, J.K., and Leutgeb, S. (2011). The spatial periodicity of grid cells is not sustained during reduced theta oscillations. Science *332*, 592–595.

Langston, R.F., Ainge, J.A., Couey, J.J., Canto, C.B., Bjerknes, T.L., Witter, M.P., Moser, E.I., and Moser, M.B. (2010). Development of the spatial representation system in the rat. Science *328*, 1576–1580.

Lever, C., Burton, S., Jeewajee, A., O'Keefe, J., and Burgess, N. (2009). Boundary vector cells in the subiculum of the hippocampal formation. J. Neurosci. *29*, 9771–9777.

McNaughton, B.L., Battaglia, F.P., Jensen, O., Moser, E.I., and Moser, M.B. (2006). Path integration and the neural basis of the 'cognitive map'. Nat. Rev. Neurosci. *7*, 663–678.

Monaco, J.D., and Abbott, L.F. (2011). Modular realignment of entorhinal grid cell activity as a basis for hippocampal remapping. J. Neurosci. *31*, 9414–9425.

Muller, R.U., and Kubie, J.L. (1989). The firing of hippocampal place cells predicts the future position of freely moving rats. J. Neurosci. *9*, 4101–4110.

O'Keefe, J., and Burgess, N. (1996). Geometric determinants of the place fields of hippocampal neurons. Nature *381*, 425–428.

O'Keefe, J., and Burgess, N. (2005). Dual phase and rate coding in hippocampal place cells: theoretical significance and relationship to entorhinal grid cells. Hippocampus *15*, 853–866.

O'Keefe, J., and Dostrovsky, J. (1971). The hippocampus as a spatial map. Preliminary evidence from unit activity in the freely-moving rat. Brain Res. *34*, 171–175.

Ranck, J.B. (1985). Head direction cells in the deep cell layer of dorsal presubiculum in freely moving rats. In Electrical Activity of the Archicortex, G. Buzsáki and C.H. Vanderwolf, eds. (Budapest: Akademiai Kiado), pp. 217–220.

Rolls, E.T., Stringer, S.M., and Elliot, T. (2006). Entorhinal cortex grid cells can map to hippocampal place cells by competitive learning. Network *17*, 447–465.

Sargolini, F., Fyhn, M., Hafting, T., McNaughton, B.L., Witter, M.P., Moser, M.-B., and Moser, E.I. (2006). Conjunctive representation of position, direction, and velocity in entorhinal cortex. Science *312*, 758–762.

Savelli, F., and Knierim, J.J. (2010). Hebbian analysis of the transformation of medial entorhinal grid-cell inputs to hippocampal place fields. J. Neurophysiol. *103*, 3167–3183.

Savelli, F., Yoganarasimha, D., and Knierim, J.J. (2008). Influence of boundary removal on the spatial representations of the medial entorhinal cortex. Hippocampus *18*, 1270–1282.

Skaggs, W.E., McNaughton, B.L., Gothard, K.M., and Markus, E.J. (1993). An information-theoretic approach to deciphering the hippocampal code. In Advances in Neural Processing Systems, *Volume 5*, S.J. Hanson, J.D. Cowan, and C.L. Giles, eds. (San Mateo: Morgan Kaufmann), pp. 1030–1037.

Skaggs, W.E., McNaughton, B.L., Wilson, M.A., and Barnes, C.A. (1996). Theta phase precession in hippocampal neuronal populations and the compression of temporal sequences. Hippocampus *6*, 149–172.

Solstad, T., Moser, E.I., and Einevoll, G.T. (2006). From grid cells to place cells: a mathematical model. Hippocampus *16*, 1026–1031.

Solstad, T., Boccara, C.N., Kropff, E., Moser, M.B., and Moser, E.I. (2008). Representation of geometric borders in the entorhinal cortex. Science *322*, 1865–1868.

Taube, J.S., Muller, R.U., and Ranck, J.B., Jr. (1990). Head-direction cells recorded from the postsubiculum in freely moving rats. I. Description and quantitative analysis. J. Neurosci. *10*, 420–435.

Wills, T.J., Cacucci, F., Burgess, N., and O'Keefe, J. (2010). Development of the hippocampal cognitive map in preweanling rats. Science *328*, 1573–1576.

Witter, M.P., and Amaral, D.G. (2004). Hippocampal formation. In The Rat Nervous System, Third Edition, G. Paxinos, ed. (San Diego: Elsevier Academic Press), pp. 635–704.

Zhang, S.J., Ye, J., Miao, C.L., Tsao, A., Cerniauskas, I., Ledergerber, D., Moser, M.B., and Moser, E.I. (2013). Optogenetic dissection of entorhinal-hippocampal functional connectivity. Science *340*, 1232627.